Published in final edited form as:
ACS Chem Biol. 2009 August 21; 4(8): 673–684. doi:10.1021/cb900112v.

Novel pentameric thiophene derivatives for *in vitro* and *in vivo* optical imaging of a plethora of protein aggregates in cerebral amyloidoses

Andreas Åslund[1], **Christina J. Sigurdson**[2], **Therése Klingstedt**[1], **Stefan Grathwohl**[3], **Tristan Bolmont**[3], **Dara L. Dickstein**[4,5], **Eirik Glimsdal**[6], **Stefan Prokop**[7], **Mikael Lindgren**[6], **Peter Konradsson**[1], **David M. Holtzman**[8], **Patrick R. Hof**[4,5], **Frank L. Heppner**[7], **Samuel Gandy**[5,9], **Mathias Jucker**[3], **Adriano Aguzzi**[2], **Per Hammarström**[1], and **K. Peter R. Nilsson**[1,2,*]

[1]Department of Chemistry, IFM, Linköping University, SE-581 83 Linköping, Sweden [2]Universitätsspital Zürich, Institute of Neuropathology, Department of Pathology, Schmelzbergstrasse 12, CH–8091 Zürich, Switzerland [3]Department of Cellular Neurology, Hertie-Institute for Clinical Brain Research, University of Tuebingen, D-72076 Tuebingen, Germany [4]Department of Neuroscience, Mount Sinai School of Medicine, New York, NY 10029, USA [5]Alzheimer's Disease Research Center, Mount Sinai School of Medicine, New York, NY, 10029, USA [6]Department of Physics, Norwegian University of Science and Technology, N-7491 Trondheim, Norway [7]Department of Neuropathology, Charité – Universitätsmedizin Berlin, D-13353 Berlin, Germany [8]Department of Neurology, Alzheimer's Disease Research Center, Washington University, St. Louis, MO, 63110, USA [9]Departments of Neurology and Psychiatry, Mount Sinai School of Medicine, New York, NY 10029, USA

Abstract

Molecular probes for selective identification of protein aggregates are important to advance our understanding of the molecular pathogenesis underlying cerebral amyloidoses. Here we report the chemical design of pentameric thiophene derivatives, denoted luminescent conjugated oligothiophenes (LCOs), which could be used for real-time visualization of cerebral protein aggregates in transgenic mouse models of neurodegenerative diseases by multiphoton microscopy. One of the LCOs, p-FTAA, showed conformation-dependent optical properties and could be utilized for *ex vivo* spectral assignment of distinct prion deposits from two mouse-adapted prion strains. p-FTAA also revealed staining of transient soluble pre-fibrillar non-thioflavinophilic Aβ- assemblies during *in vitro* fibrillation of Aβ peptides. In brain tissue samples, Aβ deposits and neurofibrillary tangles (NFTs) were readily identified by a strong fluorescence from p-FTAA and the LCO staining showed complete co-localization with conventional antibodies (6E10 and AT8), indicating that p-FTAA detects all the immuno-positive aggregated proteinaceous species in Alzheimer disease, but with significantly shorter imaging time (100 fold) compared to immunofluorescence. In addition, a patchy islet-like staining of individual Aβ plaque was unveiled by the anti-oligomer A11 antibody during co-staining with p-FTAA, suggesting that pre-fibrillar species are likely an intrinsic component of Aβ plaques in human brain. The major hallmarks of Alzheimer's disease, namely Aβ aggregates versus NFTs could also be distinguished due to distinct emission spectra from p-FTAA. Overall, we demonstrate that LCOs can be utilized as powerful practical research tools for studying protein aggregation diseases and facilitate the study of amyloid origin, evolution and maturation, Aβ−tau interactions and pathogenesis both *ex vivo* and *in vivo*.

[*]Corresponding author: K. Peter R. Nilsson, Department of Chemistry, IFM, Linköping University, SE-581 83 Linköping, Sweden, Tel.: +46 (13) 28 27 87, Fax: +46 (13) 13 75 68, petni@ifm.liu.se.

The formation of highly ordered aggregates of intra- or extracellular proteins underlies a wide range of neurodegenerative conditions including prion, Parkinson's, Huntington's and Alzheimer's (AD) diseases. Hence, molecular probes that specifically target protein aggregates and allow *in vitro* or *in vivo* imaging of these pathological hallmarks, are of great importance. Small hydrophobic probes that cross the blood-brain barrier (BBB) can be monitored *in vivo* with positron emission tomography (PET), single-photon emission computerized tomography (SPECT) or multiphoton microscopy (1-7). The latter is especially applicable in transgenic mouse models where mechanistic insights regarding the pathological events involved in the formation of protein deposits can be obtained. Additionally, molecular imaging probes may also help in early diagnosis of neurodegenerative diseases and in monitoring the effect of therapeutic interventions. However, a major drawback of these conventional probes is that only a subset of aggregates that roughly corresponds to histologically identifiable amyloid deposits can be identified, whereas several diverse types of protein aggregates, such as pre-fibrillar species and morphologically distinct fibrillar deposits, are involved in neurodegenerative diseases (8,9). In this regard, we have previously introduced luminescent conjugated polythiophenes (LCPs) as a novel class of conformation-sensitive optical probes for selective staining of protein aggregates (10-16). LCPs contain a flexible thiophene backbone and upon binding to protein aggregates the conformational freedom of the backbone is restricted, leading to specific conformation-dependent emission spectra from the LCP. This intrinsic property was recently employed to distinguish prion strains and for discrimination of heterogeneous Aβ plaques (13,14). Although, LCPs have been proven useful for resolving morphologically distinct fibrillar deposits, these molecules have limitations for being utilized as *in vivo* amyloid imaging agent and have never been shown to detect pre-fibrillar species. Hence, novel thiophene based molecular scaffold that can fulfill these criteria would be advantageous (17, 18).

Herein we report a novel class of smaller hydrophobic LCPs based on a pentameric thiophene scaffold, abbreviated LCOs (luminescent conjugated oligothiophenes). Under physiological conditions, LCOs showed a striking specificity for protein aggregates associated with prion diseases and AD. Two LCOs also crossed the BBB rather efficiently and multiphoton imaging of cerebral amyloid plaques through a cranial window in sedated beta-amyloid precursor protein (APP) transgenic mice was demonstrated. One of the LCOs revealed staining of pre-fibrillar non-thioflavinophilic Aβ-assemblies during in vitro fibrillation of Aβ peptides and was also shown to exhibit conformation-dependent spectral properties, as observed by distinct spectral signatures from the LCO bound to diverse pathological entities in human AD brain cryosections and to protein aggregates associated with distinct prion strains.

RESULTS AND DISCUSSION

Synthesis and optical characterization of luminescent conjugated oligothiophenes

Our previously reported LCPs (10-15) have rather high molecular weights (1,500-11,000 Da), carry several ionic side chain substitutions on the thiophene backbone, and hence do not fulfill the requirements for crossing the BBB. To remedy this shortcoming we designed a novel class of smaller chemically defined molecules based on a pentameric thiophene scaffold, abbreviated LCOs. The LCO, p-FTAA (Figure 1a), was designed based on the anionic LCPs, PTAA and tPTAA, and synthesized using a previously reported trimeric building block (15) (Scheme 1). To achieve molecules with diverse lipophilicity, we synthesized two additional LCOs, the methylated analogue, p-FTAM (Figure 1a), and the decarboxylated analogue p-HTAA (Figure 1a). All of the LCOs are negatively charged under physiological conditions, and the molecular weights of the three compounds range between 530-650 Da. The LCOs showed absorption and emission maxima between 380-400 nm and 515-540 nm, respectively (Supplementary Figure 1 and Supplementary Table 1). Hence, all three LCOs showed a Stokes shift of approximately

130 nm. The spectral variation between the dyes is a consequence of the chemical modifications of the substituents attached to the pentameric scaffold. p-FTAA showed a quantum efficiency (QE) around 20% and a two-photon absorption (TPA) cross-section of 20-40 GM in the wavelength range 775-850 nm (Supplementary Figures 2 and 3). Here, fluorescein in 0.1 M NaOH was used as a reference using the QE = 90% and with a TPA cross-section of 10-37 GM in the same wavelength range (19,20).

LCO binding of protein aggregates in tissue samples from transgenic mouse models

To verify selective amyloid binding of the LCOs, we stained formalin fixed brain sections from transgenic mice with AD pathology. The staining was performed with the LCOs diluted in phosphate buffer saline (PBS) and the pentameric LCOs were found to selectively stain protein deposits under these conditions (Figure 1b). The deposits were easily identified due to a bright greenish emission from the LCOs. For p-FTAA, two distinct emission peaks at 520 nm and 545 nm were observed, whereas the corresponding emission peaks of p-FTAM and p-HTAA were slightly shifted towards shorter wavelengths (Figure 1b). Additional less distinct shoulders in the range 570-630 nm were also observed for all three LCOs. The enhanced fluorescence and the well-resolved spectral substructures most likely arise from vibrational sublevels of the excited state, associated with a conformationally restricted thiophene backbone (21, 22). Similar spectral substructures have been observed for rather defined LCPs synthesized from a trimeric precursor, whereas the substructures are less defined in polydispersed LCPs (10-15). Furthermore, none of the previously reported LCPs have been found to selectively stain amyloid deposits under physiological conditions, such as PBS (12-14). The enhanced selectivity and specificity for protein aggregates observed for p-FTAA are most likely associated with an increased exposure of the hydrophobic thiophene rings, as the LCO have less ionic side chain substitution than LCPs. Increased amyloid specificity for dyes with a more exposed thiophene backbone were also recently observed in a study comparing different LCPs with the same ionic side chain functionalization but with different amounts of side chains (15).

LCOs for in vivo labeling of protein aggregates in transgenic mouse models

As the pentameric LCO probes showed selectivity for protein deposits in PBS, we next explored their ability for being used as *in vivo* imaging agents of protein aggregates in aged APP/PS1 transgenic mice with extensive Aβ deposits (23). p-FTAA and p-HTAA were dissolved in aqueous PBS (5 mg/ml), whereas p-FTAM was dissolved in DMSO (50 mg/ml) and subsequently diluted in PBS to a final concentration of 5 mg/ml. As references, we used the previously reported anionic LCPs, PTAA and tPTAA (12,15) (5 mg/ml in PBS). The mice were injected in the tail vein with 10 mg/kg of the respective LCO or LCP, and the mice were sacrificed 30 min after inoculation. In contrast to what was predicted by the chemical design of the LCOs, the most hydrophobic derivative, p-FTAM, was less efficient in crossing the BBB, whereas the fairly negatively charged p-FTAA and p-HTAA readily crossed the BBB after the intravenous injection and specifically labeled cerebral plaques (Figure 1c). This is notable as other studies have shown that development of lipophilic uncharged derivatives was required to get other conventional amyloid ligands across the BBB (2-4). It is tempting to draw the conclusion that the two acetic acid substituted thiophene moieties, which are common for p-FTAA and p-HTAA but is lacking for p-FTAM due to the esterfication of the carboxyl group, might be necessary for active transport of these LCOs over the BBB. However, it has been showed that amphipathic structures may facilitate transport across the BBB (24,25). A more extended structure-activity relationship analysis involving LCOs with diverse side chains functionalization and detail studies of the pharmacokinetic behavior of LCOs are needed to clarify this matter. Spectral analysis of the LCO-labeled deposits was also performed *ex vivo* on unfixed cryosections. Similar to the observation on LCO-stained Aβ deposits in tissue sections, two well-resolved emission peaks at 520 and 545 nm were observed for p-FTAA, and

the emission peaks of p-HTAA were slightly shifted towards shorter wavelengths (Supplementary Figure 4). As predicted, no labeling of plaques was observed in cryosections from PTAA or tPTAA injected mice.

The use of p-FTAA and p-HTAA for direct *in vivo* imaging using multiphoton microscopy were also verified with additional experiments with a cranial window installed overlying the parietal cortex of the mice (26-28). Both p-HTAA and p-FTAA specifically labeled Aβ deposits in the living brain and the *in vivo* labeling kinetics were similar for these LCOs (Supplementary Figure 4). A more detailed time-lapse study for p-HTAA is shown in figure S4e and revealed p-HTAA within minutes in the cerebral blood vessels with subsequent diffusion into the brain parenchyma. As early as 6 minutes following the injection cerebral plaques were clearly labeled by p-HTAA, verifying that this LCO crossed the BBB rather efficiently. After longer incubation periods, the background labeling (unbound compound in the brain parenchyma) was reduced and labeling was specific and limited to the cerebral plaques (Supplementary Figure 4 and supplementary movie 1). One week after injection, the mice were reexamined and intense p-FTAA and p-HTAA fluorescence from the cerebral plaques were readily detectable (Supplementary Figure 4). Hence, the LCO staining was shown to be rather persistent and as the unique emission profile allows specific identification of individual LCOs, the administration of distinct LCOs at different time points might offer the possibility to determine an indirect age of a protein deposit or for following the kinetics of aggregate formation. This will be especially useful for monitoring the results of experimental anti-aggregation AD therapies.

Previously reported LCPs have been shown to generate specific emission profiles from protein aggregates associated with distinct prion strains and from heterogenic populations of Aβ plaques (13,14). Excitingly, we found that p-FTAA was able to distinguish protein aggregates associated with distinct mouse-adapted prion strains (Figure 1d). Due to the increased specificity of LCOs for protein aggregates under physiological conditions, p-FTAA could be administered by intracerebral injection into sedated mice, allowing staining under conditions where the protein aggregates have a native structure. *Ex vivo* analysis of the prion deposits showed that p-FTAA bound to prion deposits in mice infected with mouse adapted chronic wasting disease (mCWD) emitted green light with an emission maximum around 525 nm, whereas light with a more red shifted hue (λ_{max} =550 nm) were observed from the pathological entities in mice infected with mouse adapted sheep scrapie (mSS) (Figure 1d). In contrast to the measurements on Aβ deposits, the spectral emission from p-FTAA bound to prion deposits showed broad features with no resolved vibrational substructure, indicating that p-FTAA binds in a different fashion to these prion deposits than to Aβ aggregates (Figure 1).

p-FTAA profiling of protein aggregates during fibrillation of recombinant Aβ

As p-FTAA was shown to have conformational-sensitive properties and the potential for being used as an *in vivo* amyloid imaging agent, we next investigated the photophysical properties of p-FTAA bound to amyloid fibrils made from recombinant Aβ1-42 peptide. p-FTAA bound selectively to recombinant Aβ fibrils and displayed similar well-resolved emission profiles as observed for tissue stained Aβ deposits, whereas no significant spectral changes in the spectra were observed upon mixing the pentameric thiophene derivative with freshly dissolved native Aβ1-42 peptide (Supplementary Figure 5). Hence, the backbone of p-FTAA is conformationally restricted due to selective interactions with the amyloid fibrils, leading to a distinct target-dependent fluorescence signal. Moreover, the fluorescence decaytime was increased by approximately 50% from 560 to 810 ps when bound to Aβ1-42 fibrils (Supplementary Figures 6 and 7). The conformational restriction of p-FTAA upon binding to the amyloid fibrils was even more prominent when examining the excitation spectrum (Supplementary Figure 5). The dye free in solution or mixed with freshly dissolved Aβ1-42

peptide displayed excitation spectra with a maximum around 400nm, whereas the spectrum for the dye bound to amyloid fibrils was considerably shifted towards longer wavelengths and displayed spectral substructures. The large red-shift of more than 50 nm implies that the LCO conformation upon binding to the amyloid fibril was more extended compared to the free LCO resulting in a larger transition dipole moment along the conjugated molecular framework. The apparent Stokes shift for the LCO bound to fibrils was decreased compared to the shift for LCO in solution, indicative of a restricted flexibility to relax the molecular structure upon photoexcitation. A variety of studies suggest that amyloid specific dyes bind in a thin hydrophobic groove along the long axis of the amyloid fibril and recently a similar mechanism of binding was suggested for the anionic LCP, PTAA (29, 30). p-FTAA is presumably intercalating with the amyloid fibrils through a similar mechanism and the constraints of the fibril-binding pocket are inducing unique excitation and emission pathways for the LCO.

Next we compared ThT and p-FTAA fluorescence as a read out for the formation of aggregated Aβ species during the amyloid fibrillation process. The peptides, Aβ 1-40 and Aβ 1-42, were incubated under close to physiological conditions (pH 7.5, 37°C) with repetitive cycles of agitation and with a substoichiometric amount of dye present (10 μM peptide, 0.3 μM dye). As shown in figure 2a, the fibrillation kinetics of Aβ 1-42 showed a conventional behavior, including a lag phase that was followed by a rapid exponential growth phase and a plateau phase, for both ThT and p-FTAA. As expected the rate of fibrillation of Aβ 1-40 as monitored by ThT fluorescence was slower than for Aβ 1-42, however an earlier growth phase was observed for Aβ 1-40 when the fibrillation event was monitored by p-FTAA fluorescence (Figure 2a). Hence, p-FTAA bound to non-thioflavinophilic prefibrillar species of Aβ 1-40. This phenomenon has not been seen for any of the previously reported LCPs utilized for following amyloid fibrillation *in vitro* (10, 11, 15). To explore the identity of the p-FTAA positive aggregates, the p-FTAA emission profile was correlated with transmission electron microscopy (TEM). For Aβ 1-40, the spectrum of p-FTAA was already altered after 120 min of incubation, seen as an increased emission and characteristic well-resolved vibronic structures, and TEM analysis revealed a homogenous population of small spherical aggregates of Aβ (Figure 2b, left). At the end of the earlier lag phase observed by p-FTAA, a mixture of small spherical aggregates and fibrils were presented in the sample, whereas at 600 min when both ThT and p-FTAA emission showed a plateau phase, only mature fibrils were observed by TEM (Figure 2b). Hence, p-FTAA interacts with non-thioflavinophilic spherical aggregates of Aβ 1-40 that can be visualized by TEM. On the other hand, the TEM analysis of Aβ 1-42 at analogous time points, i.e. in the beginning (100 min) and the middle of the growth phase (200 min) or during the plateau phase (600 min), showed a mixture of small spherical aggregates and fibrils (100 min) or mature fibrils (200 and 600 min) (Figure 2c). Thus, a homogenous population of small spherical aggregates was not observed at any distinct time point, suggesting that the conversion of the small spherical aggregates to fibrils occurred more rapidly for Aβ 1-42 than for Aβ 1-40. This conclusion is congruent with the emission profile from both ThT and p-FTAA, as the fibrillation kinetics of Aβ 1-42 were similar using both dyes (Figure 2a).

To rule out the possibility that p-FTAA accelerated the fibrillation kinetics of Aβ 1-40, amyloid fibrillation without the presence of any dye was analyzed with p-FTAA and ThT at different time points. Prefibrillar non-thioflavinophilic Aβ aggregates were still observable with p-FTAA fluorescence using this experimental set up, verifying that p-FTAA did not accelerate the fibrillation rate at the concentration used (Supplementary Figure 8). Additionally the analyzed samples were centrifuged at 16 000 g for 30 min and the p-FTAA emission was similar before and after centrifugation in the sample containing the pre-fibrillar aggregates, indicating that these Aβ species are soluble. In contrast, ThT and p-FTAA positive samples assayed at a later time point (near the plateau phase) showed a substantial decreased emission after centrifugation (Supplementary Figure 8). Overall, the above findings underline the new

tantalizing possibilities for using p-FTAA as a probe for studying *in vitro* fibrillation of different Aβ peptides as well as other amyloidogenic proteins.

p-FTAA profiling of protein aggregates in human AD brain tissue

The high selectivity of p-FTAA for protein aggregates was further demonstrated by performing histochemical staining of cryosections from human cases with AD pathology. Since recent studies have shown that lightly fixed cryosections are the preferable choice to achieve optimal spectral resolution and improved binding of LCPs, the sections were briefly fixed in ethanol for 10 min (13,14). After staining in PBS, extensive p-FTAA staining was only observed in the same areas of the samples that were positive for 6E10 (monoclonal antibody for Aβ) and AT8 (monoclonal antibody for hyperphosphorylated tau, position 202 and 205, neurofibrillary tangles, NFTs) immunohistochemistry, whereas areas without AD pathology were negative for p-FTAA staining (Supplementary Figure 9). Aβ deposits, NFTs and other pathological structures associated with AD, such as dystrophic neurites were readily identified by a strong fluorescence from p-FTAA and the LCO staining showed complete co-localization with both 6E10 and AT8 (Figure 3a-b). The imaging time of p-FTAA stained aggregates was reduced (100 fold) compared to immunofluorescence and less photobleaching was also observed from the LCO labelled deposits. The LCOs were also tried on formalin-fixed sections from human cases with AD pathology. All LCO staining revealed selective and specific staining of both cortical plaques and cerebrovascular amyloid (Supplementary Figure 10). However, presumably due to the harsh fixation of the tissue, the staining of intracellular protein aggregates, such as NFTs, were almost completely abolished in these sections.

As p-FTAA was shown to bind small spherical aggregated species of Aβ *in vitro*, we subsequently correlated the p-FTAA staining in the human AD brain tissue with a conventional oligomer specific Aβ antibody, A11 (31,32). In contrast to the staining with 6E10, which showed complete co-localization, the p-FTAA stained Aβ deposits only showed partial co-localization with A11 staining (Figure 3c). In apparent contradiction to what has been reported previously (32), this co-localization was seen at certain nodes inside the deposits and not as a halo surrounding the amyloid plaque. However, in the earlier study (32) an oligomeric/amyloid fibril specific antibody, NAB61, was used (33). In addition, several different forms and sizes of oligomeric species of Aβ, which reacts with specific antibodies, have been reported (31-35). Some of these studies (31,35) have also suggested that distinct oligomeric species are found at locations separated from the plaques. Hence, it is an on-going debate regarding the localization and the molecular composition of the presumably toxic oligomeric Aβ species seen in AD. Taken together our data shows that p-FTAA, under the conditions used herein (mild fixation for preserving the structure of the aggregates), stains all the aggregated Aβ species that are observed by conventional commercially available immunofluorescence reagents (6E10 and A11) and notably p-FTAA seems to provide two magnitudes better signal to noise ratio than conventional immunofluorescence. Thus, p-FTAA can be utilized as a small-molecular dye for studying various Aβ aggregates and such a dye will be highly significant for mapping heterogeneous aggregated species of Aβ in combination with existing antibodies.

When performing spectral analysis of the human brain tissue samples, we found that protein aggregates associated with distinct pathological entities observed in AD displayed distinct p-FTAA spectra. p-FTAA bound to Aβ deposits emitted green light with two similar emission peaks (λ_{max} =520 and 545 nm), whereas light with a more red shifted hue (λ_{max} =558 nm) were observed from the pathological entities associated with aggregated tau protein, such as NFTs and dystrophic neurites (Figure 4). This phenomenon was not observed for any of the other LCOs or the polymeric counterpart, PTAA (Supplementary Figure 11). Hence, the positioning of the anionic carboxylic groups and the amount of net charge on the thiophene backbone seems to be important factors for obtaining optimal spectral discrimination of protein aggregates of

diverse origin. Removing the charge from the acetic acid substitutions at position number 3 on thiophene rings 2 and 4 (p-FTAM) or removing the formic acid groups at position number 2 on thiophene rings 1 and 5 (p-HTAA) from the pentameric thiophene scaffold will abolish the spectral phenomenon seen for p-FTAA bound to Aβ and tau aggregates. Similarly, addition of more negative groups and extension of the thiophene backbone (PTAA) will also abolish the spectral distinction of these aggregates. Overall, the maintenance of the unique conformational-dependent optical properties for p-FTAA opens up the possibility for a wide range of appealing experiments. As shown in figure 4, high resolution fluorescence images collected with a SpectraCube® module using a long pass filter for excitation (Figures 4a, 4b and 4d) or a combination of two long pass filters (Figure 4e), both provide sufficient structural details and allow distinct spectral separation of these pathological hallmarks seen in AD. Aβ aggregates are clearly visible in green, whereas other entities, corresponding to dystrophic neurites and NFTs, exhibit yellow-red fluorescence. Thus, the distinctive spectral signatures from p-FTAA bound to Aβ aggregates or tau deposits can be used to study the interplay between these entities in more detail. Distinguishing protein deposits of diverse origin are of great interest and LCOs may be utilized to resolve and clarify the importance of amyloid cross-seeding as a disease mechanism. The latter is of great importance as a diversity of amyloidogenic proteins have shown to form fibrillar aggregates through a nucleation-dependent aggregation process that can be initiated or seeded by a pathogenic mechanism resembling prions (36-39).

In conclusion, we have presented a novel molecular scaffold, the LCOs, which can be utilized for specific labeling of protein aggregates. The ability to cross the BBB combined with the unique spectral properties of the LCOs, especially p-FTAA, makes them unique compared to other small amyloid ligands. Furthermore, p-FTAA was found to detect pre-fibrillar nonthioflavinophilic Aβ-assemblies. Clearly, the practical application of the pentameric thiophenes in diagnostics and in truly noninvasive monitoring of the brain surface, require the synthesis of modified LCO analogues for PET, SPECT or magnetic resonance (MR) imaging. Nonetheless, these luminescent oligothiophene derivatives show a remarkable specificity for a plethora of protein aggregates and provide unique optical properties suitable for achieving real-time mechanistic insight into the protein aggregation process and the molecular pathology of protein aggregation disorders. We foresee that these probes will offer practical research tools for studying protein aggregation diseases and facilitate the study of amyloid origin and pathogenesis *in vitro* and in animal models.

Methods

Synthesis of the LCOs

The detailed synthesis of p-FTAA, p-FTAM and p-FTAA are shown in the supplementary material and in scheme 1. Briefly, all of the LCO were synthesized by iodination of a trimeric thiophene precursor (**1**) (15). The iodinated trimer (**2**) was further converted to pentamers by addition of 2-thiopheneboronic acid or 5-(dihydroxyboryl)-2-thiophenecarboxylic through Suzuki coupling (**3**, p-FTAM (**5**)). The methyl group was removed by NaOH to achieve p-HTAA (**4**) and p-FTAA (**6**). p-HTAA and p-FTAA was converted to its corresponding sodium salt by dissolving it in H_2O and equimolar amounts of sodium hydroxide, relative the number of carboxylic acids.

In vivo imaging of Aβ deposits in the brain of transgenic APP/PS1 mice

Transgenic APP/PS1 mice were aged for 10-11 months. Two days before imaging, a round cranial window (5 mm length) was created under isoflurane anesthesia as described (28). After surgery, mice were treated with Temgesic (0.05 mg/kg intraperitonally daily; Essex Pharma GmbH, Munich) for 3 consecutive days. Before imaging, mice were anesthetized with isoflurane (induction with 5% and then reduced to 1%). Mice were then attached to a custom

build head fixation, and the window was cleaned with ethanol immediately before imaging. Mice were injected intravenously with 10 mg/kg of the respective LCO (5 mg/ml in PBS). Imaging was performed with a 40x water immersion lens (0.8 numerical aperture, U-V-I 0/D; Leica Microsystems, Bensheim, Germany). Multiphoton excitation at 910 nm was generated by a Spectra Physics (San Jose, CA) Mai-Tai laser (tunable 770–990 nm) and for detection two non-descanned detectors (R6357 P.M.T.; Hamamatsu, Bridgewater, NJ) were used at close proximity to the objective lens. Visualization of the LCO fluorescence was performed via a FITC/tetramethylrhodamine isothiocyanate filter (reflection short pass, 560; bandpass, 525/50; bandpass, 610/75). Two different xyz stacks were recorded per mouse. Positions were chosen containing a large blood vessel and several amyloid plaques.

Kinetic measurement of recombinant Aβ peptide fibrillation

In vitro amyloid fibrils were prepared by solubilization of recombinant Aβ1–42 or Aβ1-40 (rPeptide, lyophilized from hexafluoreo iso-propanol) (10 μM) in 10 mM Na-phosphate pH 7.5. After addition of the respective dye, p-FTAA (1.5 mM in de-oinized water) or ThT (2 mM in de-ionized water), to a final concentraion of 0.3 μM, the samples were incubated at 37 °C with repetivive cycles of agitation (8 min agitation, 12 min stagnant sample read) in a Tecan Saphire 2 plate reader. Spectra were collected between 470-700 nm using with excitation at 450 nm.

Co-staining with LCO and antibody on human brain cryosections with AD pathology

Immunohistochemical staining was carried out on frozen brain sections from AD patients. The sections were fixed in acetone for 10 minutes and then allowed to dry. Oligomers, amyloid deposits or phosphorylated tau were immunolabeled with A11 polyclonal antibody (1:200, Chemicon International, Temecula, CA, USA), 6E10 monoclonal antibody (1:100, Covance, Princeton, NJ, USA) or AT8 monoclonal antibody (1:100, Innogenetics, Gent, Belgium), respectively. The primary antibodies were diluted in PBS and incubated with the sections for 1 h at RT. After washing with PBS, the 6E10 and AT8 antibodies were detected by incubation in Alexa Fluor 594-conjugated Goat Anti-Mouse IgG (1:400, Molecular Probes, Eugene, OR, USA) and the A11 antibody was detected by incubation with Red-X-AffiniPure Donkey Anti-Mouse IgG (1:250, Jackson ImmunoResearch Europe Ltd., UK) for 30 minutes at RT. Thereafter, the sections were washed in PBS and incubated with p-FTAA (1.5 mM in de-ionized water), diluted 1:500 in PBS, for 30 minutes at RT. After rinsing with PBS, the sections were mounted with Dako mounting solution for fluorescence (Dako, Glostrup, Danmark). The fluorescence from the tissue samples was recorded with an epifluorescence microscope (Zeiss Axiovert A200 Mot inverted microscope) equipped with a SpectraCube® (Optical head) module, through a 470/40 nm bandpass filter (LP515), and a 546/12 nm bandpass filter (LP590). The presentation of images was achieved with the standard software (SpectraView™).

LCO staining of human brain cryosections with AD pathology

Cryosections were fixed in absolute ethanol for 10 min and rehydrated in water followed by PBS. Stock solutions of the pentameric LCPs (1.5 mM) were diluted to a final concentration of 30 μM in PBS and added to the brain sections, which were then incubated for 30 min at room temperature and washed with PBS. The sections were mounted with Dakocytocrom fluorescent mounting medium (Dako, Denmark). The fluorescence from the tissue samples was recorded as described above. Spectra were recorded with an LSM 510 META (Carl Zeiss, Jena, Germany) confocal laser scanning microscope through Plan-Neofluar 40L/0.75 objectives with an excitation at 458 nm. The selection of spectral regions and spectral processing were achieved with the standard software (LSM Image browser).

Supplementary Material

Refer to Web version on PubMed Central for supplementary material.

Acknowledgments

Our work is supported by the Swedish Foundation for Strategic Research (K.P.R.N, P.H., P.K. and A.Å.), the Knut and Alice Wallenberg foundation (K.P.R.N., P.H.), the Swedish Research Council (P.H., P.K, A.Å), the US National Prion Research Program (CJS), the German National Genome Network (BMBF-NGFNPlus, M.J.), the German Competence Network on Degenerative Dementias (M.J.), the Deutsche Forschungsgemeinschaft (SFB TRR43, F.L.H) and the US National Institutes of Health (NS046006, F.L.H.; AG02219 and AG05138, D.L.D., P.R.H., S.G.; AG005681, D.M.H; and NS055116, C.J.S). Human brain tissue was obtained from the Washington University Alzheimer's Disease Research Center, (St. Louis, MO, USA, NIH P50-AG005681, D.M.H) Center and from the Mount Sinai School of Medicine Alzheimer's Disease Research Center (New York, NY, USA). A generous gift from Astrid and Georg Olsson is also gratefully acknowledged. A.Å. is enrolled in the doctoral program Forum Scientum and P.H. is a Swedish Royal Academy of Science Research Fellow sponsored by a grant from the Knut and Alice Wallenberg Foundation. We thank S. Fransson (Universitätsspital, Zürich, Switzerland), I. Berg (Linköping University, Linköping, Sweden) and W.G.M. Janssen (Mount Sinai School of Medicine, New York, USA) for providing technical support.

References

1. DeKosky ST, Marek K. Looking backward to move forward: early detection of neurodegenerative disorders. Science 2003;302:830–834. [PubMed: 14593169]
2. Klunk WE, Bacskai BJ, Mathis CA, Kajdasz ST, McLellan ME, Frosch MP, Debnath ML, Holt DP, Wang Y, Hyman BT. Imaging Abeta plaques in living transgenic mice with multiphoton microscopy and methoxy-X04, a systemically administered Congo red derivative. J Neuropathol Exp Neurol 2002;61:797–805. [PubMed: 12230326]
3. Nesterov EE, Skoch J, Hyman BT, Klunk WE, Bacskai BJ, Swager TM. In vivo optical imaging of amyloid aggregates in brain: design of fluorescent markers. Angew Chem Int Ed 2005;44:5452–5456.
4. Mathis CA, Bacskai BJ, Kajdasz ST, McLellan ME, Frosch MP, Hyman BT, Holt DP, Wang Y, Huang GF, Debnath ML, Klunk WE. A lipophilic thioflavin-T derivative for positron emission tomography (PET) imaging of amyloid in brain. Bioorg Med Chem Lett 2002;12:295–298. [PubMed: 11814781]
5. Kung MP, Hou C, Zhuang ZP, Skovronsky DM, Zhang B, Gur TL, Trojanowski JQ, Lee VM, Kung HF. Radioiodinated styrylbenzene derivatives as potential SPECT imaging agents for amyloid plaque detection in Alzheimer's disease. J Mol Neurosci 2002;19:7–10. [PubMed: 12212796]
6. Klunk WE, Engler H, Nordberg A, Wang Y, Blomqvist G, Holt DP, Bergström M, Savitcheva I, Huang GF, Estrada S, Ausén B, Debnath ML, Barletta J, Price JC, Sandell J, Lopresti BJ, Wall A, Koivisto P, Antoni G, Mathis CA, Långström B. Imaging brain amyloid in Alzheimer's disease with Pittsburgh Compound-B. Ann Neurol 2004;55:306–319. [PubMed: 14991808]
7. Zhang W, Oya S, Kung MP, Hou C, Maier DL, Kung HF. F-18 stilbenes as PET imaging agents for detecting beta-amyloid plaques in the brain. J Med Chem 2005;48:5980–5988. [PubMed: 16162001]
8. Chiti F, Dobson CM. Protein misfolding, functional amyloid, and human disease. Annu Rev Biochem 2006;75:333–366. [PubMed: 16756495]
9. Haass C, Selkoe DJ. Soluble protein oligomers in neurodegeneration: lessons from the Alzheimer's amyloid beta-peptide. Nat Rev Mol Cell Biol 2007;8:101–112. [PubMed: 17245412]
10. Nilsson KPR, Herland A, Hammarström P, Inganäs O. Conjugated polyelectrolytes: conformation-sensitive optical probes for detection of amyloid fibril formation. Biochemistry 2005;44:3718–3724. [PubMed: 15751948]
11. Herland A, Nilsson KPR, Olsson JDM, Hammarström P, Konradsson P, Inganäs O. Synthesis of a regioregular zwitterionic conjugated oligoelectrolyte, usable as an optical probe for detection of amyloid fibril formation at acidic pH. J Am Chem Soc 2005;127:2317–2323. [PubMed: 15713111]
12. Nilsson KPR, Hammarström P, Ahlgren F, Herland A, Schnell EA, Lindgren M, Westermark GT, Inganäs O. Conjugated polyelectrolytes—conformation-sensitive optical probes for staining and characterization of amyloid deposits. ChemBioChem 2006;7:1096–1104. [PubMed: 16729336]
13. Nilsson KPR, Åslund A, Berg I, Nyström S, Konradsson P, Herland A, Inganäs O, Stabo-Eeg F, Lindgren M, Westermark GT, Lannfelt L, Nilsson LNG, Hammarström P. Imaging Distinct

conformational states of amyloid-β fibrils in Alzheimer's disease using novel luminescent probes. ACS Chem Biol 2007;2:553–560. [PubMed: 17672509]

14. Sigurdson CJ, Nilsson KPR, Hornemann S, Manco G, Polymenidou M, Schwarz P, Leclerc M, Hammarström P, Wüthrich K, Aguzzi A. Prion strain discrimination using luminescent conjugated polymers. Nat Methods 2007;4:1023–1030. [PubMed: 18026110]
15. Åslund A, Herland A, Hammarström P, Nilsson KPR, Jonsson B-H, Inganäs O, Konradsson P. Studies of luminescent conjugated polythiophene derivatives: enhanced spectral discrimination of protein conformational states. Bioconjug Chem 2007;18:1860–1868. [PubMed: 17939727]
16. Sigurdson CJ, Nilsson KPR, Hornemann S, Heikenwalder M, Manco G, Schwarz P, Ott D, Rülicke T, Liberski PP, Julius C, Falsig J, Stitz L, Wüthrich K, Aguzzi A. De novo generation of a transmissible spongiform encephalopathy by mouse transgenesis. Proc Natl Acad Sci U S A 2009;106:304–309. [PubMed: 19073920]
17. Stains CI, Ghosh I. When conjugated polymers meet amyloid fibrils. ACS Chem Biol 2007;2:525–528. [PubMed: 17708668]
18. Jackson WS, Lindquist S. Illuminating aggregate heterogeneity in neurodegenerative disease. Nat Methods 2007;4:1000–1001. [PubMed: 18049468]
19. Damas JN, Crosby GA. Measurement of photoluminescence quantum yields. J Phys Chem 1971;75:991–1024.
20. Albota MA, Xu C, Webb WW. Two-Photon Fluorescence Excitation Cross Sections of Biomolecular Probes from 690 to 960 nm. Appl Opt 1998;37:7352–7356. [PubMed: 18301569]
21. Voropai ES, Samtsov MP, Kaplevskii KN, Maskevich AA, Stepuro VI, Povarova OI, Kuznetsova IM, Turoverov KK, Fink AL, Uverskii VN. Spectral properties of thioflavin T and its complexes with amyloid fibrils. Spectral Properties of Thioflavin T and Its Complexes with Amyloid Fibrils. J Appl Spectrosc 2003;70:868–874.
22. Stabo-Eeg F, Lindgren M, Nilsson KPR, Inganäs O, Hammarström P. Quantum efficiency and two-photon absorption cross-section of conjugated polyelectrolytes used for protein conformation measurements with applications on amyloid structures. Chem Phys 2007;336:121–126.
23. Radde R, Bolmont T, Kaeser SA, Coomaraswamy J, Lindau D, Stoltze L, Calhoun ME, Jäggi F, Wolburg H, Gengler S, Haass C, Ghetti B, Czech C, Hölscher C, Mathews PM, Jucker M. Abeta42-driven cerebral amyloidosis in transgenic mice reveals early and robust pathology. EMBO Rep 2006;7:940–946. [PubMed: 16906128]
24. Polt R, Porreca F, Szabò LZ, Bilsky EJ, Davis P, Abbruscato TJ, Davis TP, Harvath R, Yamamura HI, Hruby VJ. Glycopeptide enkephalin analogues produce analgesia in mice: evidence for penetration of the blood-brain barrier. Proc Natl Acad Sci U S A 1994;91:7114–7118. [PubMed: 8041755]
25. Dhanasekaran M, Palian MM, Alves I, Yeomans L, Keyari CM, Davis P, Bilsky EJ, Egleton RD, Yamamura HI, Jacobsen NE, Tollin G, Hruby VJ, Porreca F, Polt R. Glycopeptides related to beta-endorphin adopt helical amphipathic conformations in the presence of lipid bilayers. J Am Chem Soc 2005;127:5435–5448. [PubMed: 15826181]
26. Denk W, Strickler JH, Webb WW. Two-photon laser scanning fluorescence microscopy. Science 1990;248:73–76. [PubMed: 2321027]
27. Becker A, Hessenius C, Licha K, Ebert B, Sukowski U, Semmler W, Wiedenmann B, Grötzinger C. Receptor-targeted optical imaging of tumors with near-infrared fluorescent ligands. Nat Biotechnol 2001;19:327–331. [PubMed: 11283589]
28. Bolmont T, Haiss F, Eicke D, Radde R, Mathis CA, Klunk WE, Kohsaka S, Jucker M, Calhoun ME. Dynamics of the microglial/amyloid interaction indicate a role in plaque maintenance. J Neurosci 2008;28:4283–4292. [PubMed: 18417708]
29. Groenning M, Norrman M, Flink JM, van de Weert M, Bukrinsky JT, Schluckebier G, Frokjaer S. Binding mode of Thioflavin T in insulin amyloid fibrils. J Struct Biol 2007;159:483–497. [PubMed: 17681791]
30. Herland A, Björk P, Hania PR, Scheblykin IG, Inganäs O. Alignment of a conjugated polymer onto amyloid-like protein fibrils. Small 2007;3:318–325. [PubMed: 17262758]

31. Kayed R, Head E, Thompson JL, McIntire TM, Milton SC, Cotman CW, Glabe CG. Common structure of soluble amyloid oligomers implies common mechanism of pathogenesis. Science 2003;300:486–489. [PubMed: 12702875]
32. Koffie RM, Meyer-Luehmann M, Hashimoto T, Adams KW, Mielke ML, Garcia-Alloza M, Micheva KD, Smith SJ, Kim ML, Lee VM, Hyman BT, Spires-Jones TL. Oligomeric amyloid beta associates with postsynaptic densities and correlates with excitatory synapse loss near senile plaques. Proc Natl Acad Sci U S A 2009;106:4012–4017. [PubMed: 19228947]
33. Lee EB, Leng LZ, Zhang B, Kwong L, Trojanowski JQ, Abel T, Lee VM. Targeting amyloid-beta peptide (Abeta) oligomers by passive immunization with a conformation-selective monoclonal antibody improves learning and memory in Abeta precursor protein (APP) transgenic mice. J Biol Chem 2006;281:4292–4299. [PubMed: 16361260]
34. Wang XP, Zhang JH, Wang YJ, Feng Y, Zhang X, Sun XX, Li JL, Du XT, Lambert MP, Yang SG, Zhao M, Klein WL, Liu RT. Conformation-dependent single-chain variable fragment antibodies specifically recognize beta-amyloid oligomers. FEBS Lett 2009;583:579–584. [PubMed: 19162022]
35. Lesné S, Koh MT, Kotilinek L, Kayed R, Glabe CG, Yang A, Gallagher M, Ashe KH. A specific amyloid-beta protein assembly in the brain impairs memory. Nature 2006;440:352–357. [PubMed: 16541076]
36. Kane MD, Lipinski WJ, Callahan MJ, Bian F, Durham RA, Schwarz RD, Roher AE, Walker LC. Evidence for seeding of beta -amyloid by intracerebral infusion of Alzheimer brain extracts in beta -amyloid precursor protein-transgenic mice. J Neurosci 2000;20:3606–3611. [PubMed: 10804202]
37. Lundmark K, Westermark GT, Nyström S, Murphy CL, Solomon A, Westermark P. Transmissibility of systemic amyloidosis by a prion-like mechanism. Proc Natl Acad Sci U S A 2002;102:6979–6984. [PubMed: 12011456]
38. Lundmark K, Westermark GT, Olsén A, Westermark P. Protein fibrils in nature can enhance amyloid protein A amyloidosis in mice: Cross-seeding as a disease mechanism. Proc Natl Acad Sci U S A 2005;102:6098–6102. [PubMed: 15829582]
39. Meyer-Luehmann M, Coomaraswamy J, Bolmont T, Kaeser S, Schaefer C, Kilger E, Neuenschwander A, Abramowski D, Frey P, Jaton AL, Vigouret JM, Paganetti P, Walsh DM, Mathews PM, Ghiso J, Staufenbiel M, Walker LC, Jucker M. Exogenous induction of cerebral beta-amyloidogenesis is governed by agent and host. Science 2006;313:1781–1784. [PubMed: 16990547]

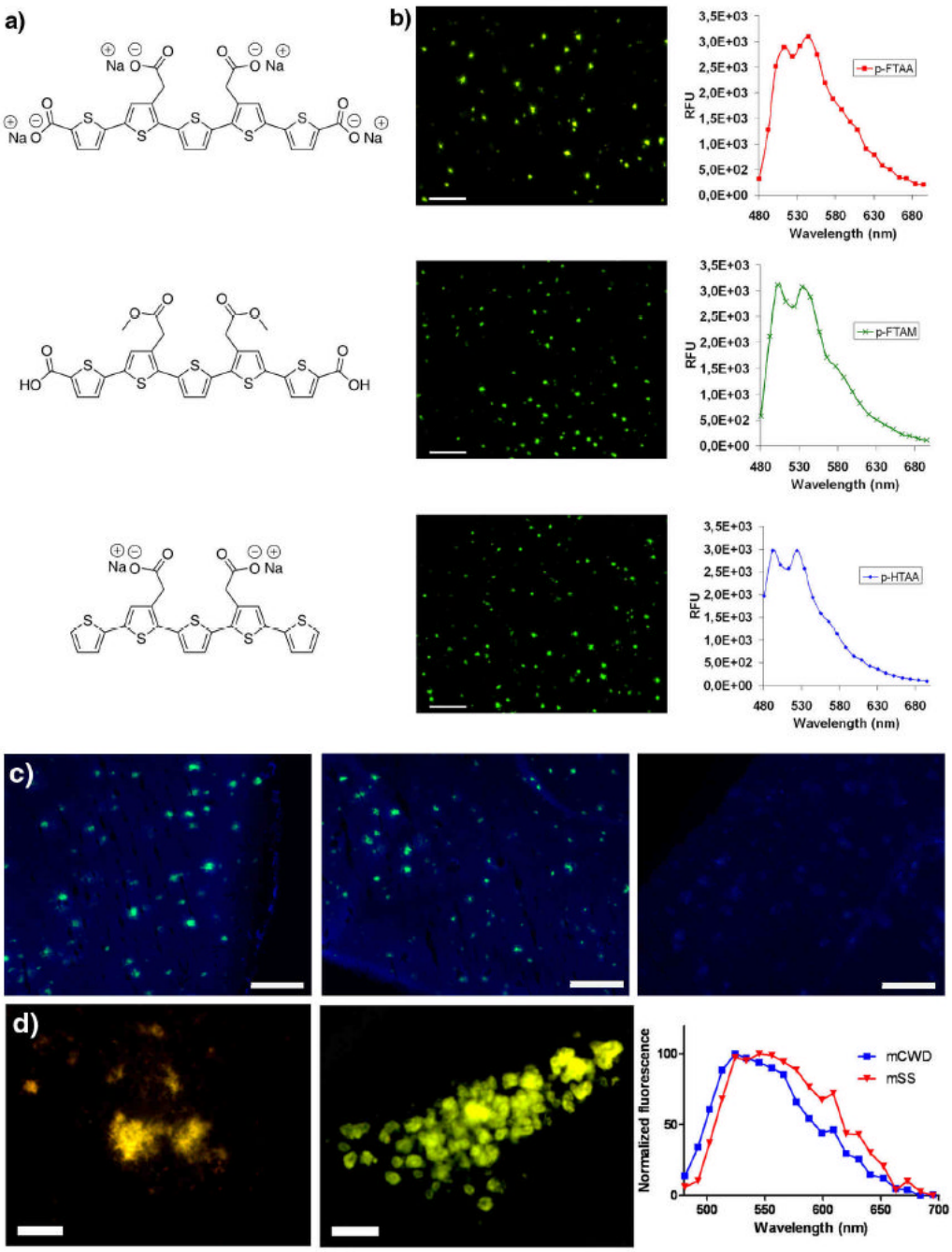

Figure 1. Chemical structures, emission spectra and fluorescence images of the pentameric LCPs upon binding to Aβ deposits in formalin-fixed tissue samples fromttransgenic mice with AD pathology, and *ex vivo* imaging of protein deposits in mice after intravenous or intracerebral injections with LCOs

a) Chemical structure of the sodium salt of pentamer formyl thiophene acetic acid (p-FTAA, top), pentamer formyl thiophene acetic methyl (p-FTAM, middle) and the sodium salt of pentamer hydrogen thiophene acetic acid (p-HTAA). **b)** Fluorescence images and emission spectra of Aβ deposits in tissue sections from APP/PS1 transgenic mice labeled by p-FTAA (top), p-FTAM (middle) or p-HTAA (bottom). All of the stains were performed with the LCOs diluted in PBS. Scale bars = 200 μm. **c)** *Ex vivo* fluorescence images of cerebral amyloid

plaques in brain crysosections from APP/PS1 mice that have been intavenously injected with p-FTAA (top), p-FTAM (middle) and p-HTAA (bottom). The images were recorded using a blue filter (LP 450) and a green filter (LP 515). After the i.v. injection of p-FTAA and p-HTAA the staining of the Aβ deposits are seen in characteristic green color, whereas upon injection of p-FTAM only blue autofluorescence from the deposits and the background are observed. Scale bars = 200 μm. **d)** *Ex vivo* fluorescence image of p-FTAA-labeled prion deposits in mice infected with mouse-adapted sheep scrapie, mSS (left) or mouse-adapted chronic wasting disease, mCWD (middle) that have been intracerebrally injected with p-FTAA. Typical emission spectra from p-FTAA (bottom) upon binding to mCWD (blue) or mSS (red) deposits. Scale bars represent 50 μm.

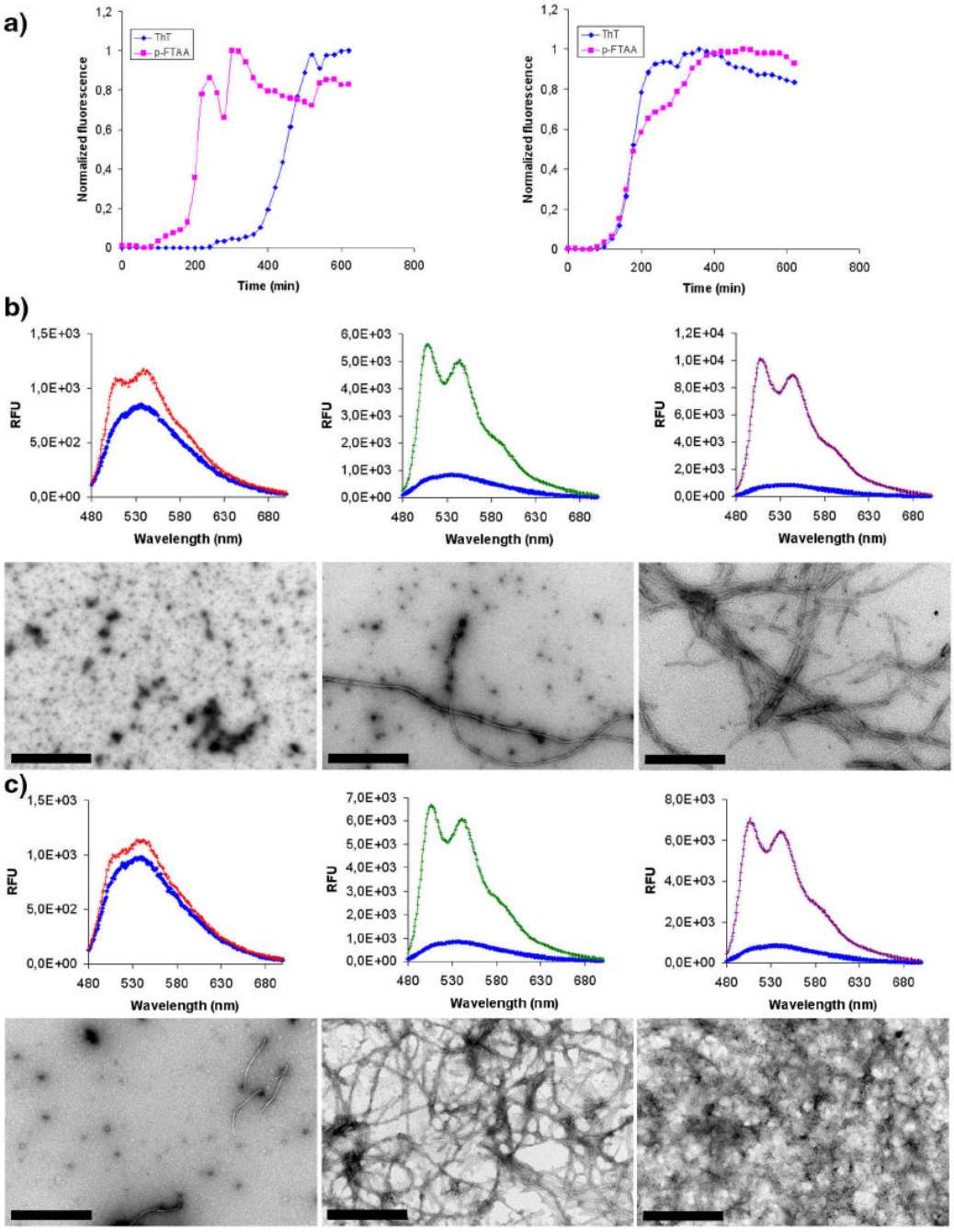

Figure 2. Recombinant Aβ 1-40 and Aβ 1-42 fibrillation monitored with ThT or p-FTAA fluorescence and TEM

a) Time plots of the kinetics of recombinant Aβ 1-40 (left) and Aβ 1-42 (right) fibrillation monitored by ThT fluorescence (blue) or p-FTAA fluorescnce (magenta). For Aβ 1-42 both of the dyes showed similar kinetics, whereas p-FTAA reacts much earlier than ThT during the fibrillation of Aβ 1-40. **b)** Fluorescence spectra of p-FTAA and the corresponding TEM micrographs after 120 min (left), 220 min (middle) and 600 min of Aβ 1-40 fibrillation. A high amount of smaller oligomeric species are present at 120 min, whereas a mixture of oligomers and fibrils are observed after 220 min. At 600 min only matured fibrils are observed. **c)** Fluorescence spectra of p-FTAA and the corresponding TEM micrographs after 100 min (left),

200 min (middle) and 600 min of Aβ 1-42 fibrillation. A small amount of smaller oligomeric species and fibrils are present at 100 min, whereas mature fibrils are observed at both 200 min and 600 min. The fibrillation experiments were performed in 10 mM Na-phosphate pH 7.5 with repetitive agitation with a concentration of 10 μM Aβ peptide and 0.3 μM of the respective dye present during fibrillation.

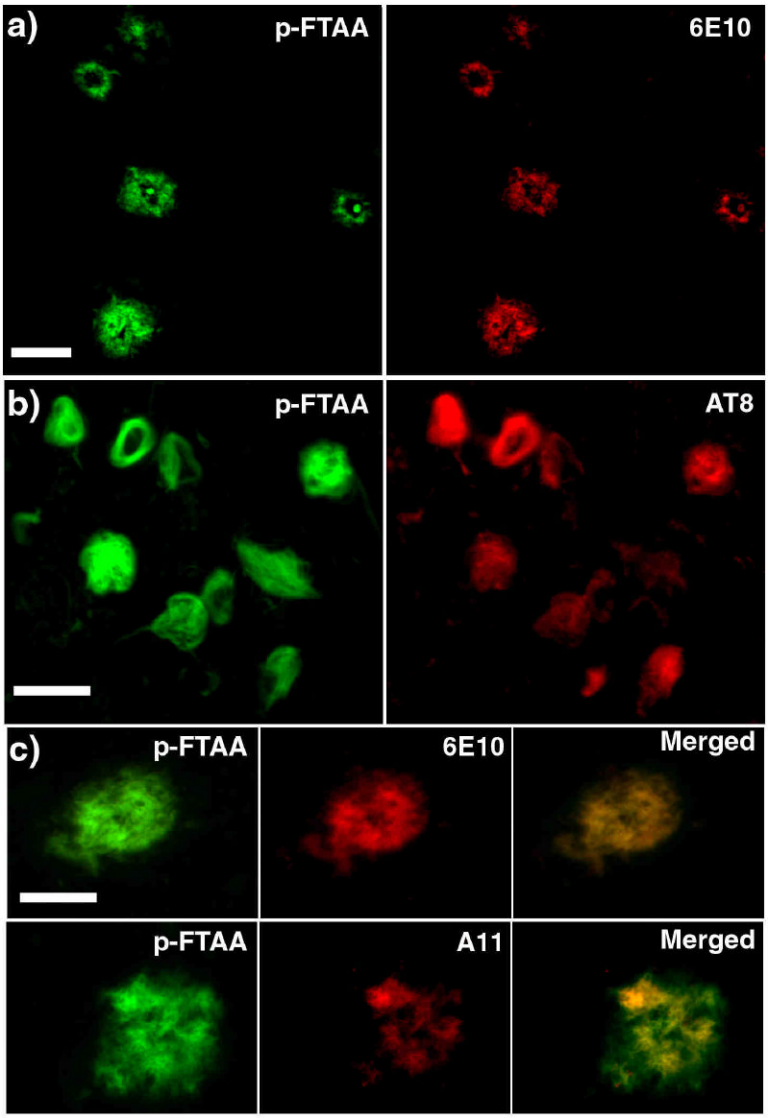

Figure 3. Fluorescence images showing the co-localization of conventional immunohistochemical dyes and p-FTAA bound to pathogenic hallmarks in human AD tissue sections

a) Fluorescence images showing an overview of Aβ deposits stained by p-FTAA (green) and 6E10 (Aβ amyloid) (red). Scale bar represent 50 μm **b)** Fluorescence images showing an overview of NFTs stained by p-FTAA (green) and AT8 (NFTs) (red). Scale bar represent 20 μm **c)** High magnification fluorescence images comparing Aβ deposits stained by p-FTAA (green) and 6E10 (red) or p-FTAA (green) and A11 (oligomeric Aβ) (red). The p-FTAA and 6E10 shows perfect co-localization, whereas the A11 only partially co-localize with the p-FTAA staining. Scale bar represent 20 μm. The p-FTAA and the corresponding antibody staining were performed on the same sections. All the images were recorded with an epifluorescence microscope (Zeiss Axiovert A200 Mot inverted microscope) equipped with a SpectraCube® (Optical head) module, using a combination of a 470/40 nm bandpass filter (LP515) and a 546/12 nm bandpass filter (LP590). The integration time used for recording these images were typically 1-5 ms for p-FTAA and 100-500 ms for the antibodies, indicating a superior sensitivity for the LCO compared to immunofluorescence.

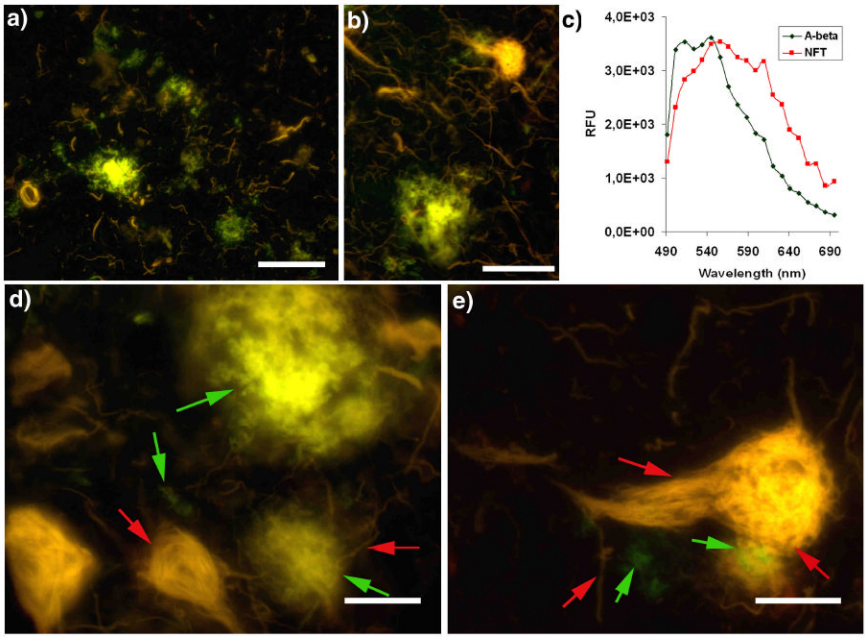

Figure 4. High resolution fluorescence images and emission spectra of p-FTAA bound to pathogenic hallmarks in AD

a-b) High resolution fluorescence images showing an overview of the interplay between Aβ deposits (green), neurofibrillary tangles (NFTs) and dystrophic neurites (yellow red). **c)** Emission spectra of p-FTAA bond to Aβ aggregates (green spectrum) or NFTs (red spectrum). Spectra were recorded with an LSM 510 META (Carl Zeiss, Jena, Germany) confocal laser scanning **d-e)** High resolution fluorescence images showing the details of the interplay between Aβ deposits (green), neurofibrillary tangles (NFTs) and dystrophic neurites (yellow red). Selected Aβ deposits and neurofibrillary tangles (NFTs), are highlighted (green and red arrows, respectively) to indicate striking spacial co-localization. All the images were recorded with an epifluorescence microscope (Zeiss Axiovert A200 Mot inverted microscope) equipped with a SpectraCube® (Optical head) module, using a 470/40 nm bandpass filter (LP515) (Image **a, b, d**), or a combination of a 470/40 nm bandpass filter (LP515) and a 546/12 nm bandpass filter (LP590) (Image **e)**. Scale bar = 50 μm (**a**), 20 μm (**b**) and 10 μm (**d-e**).

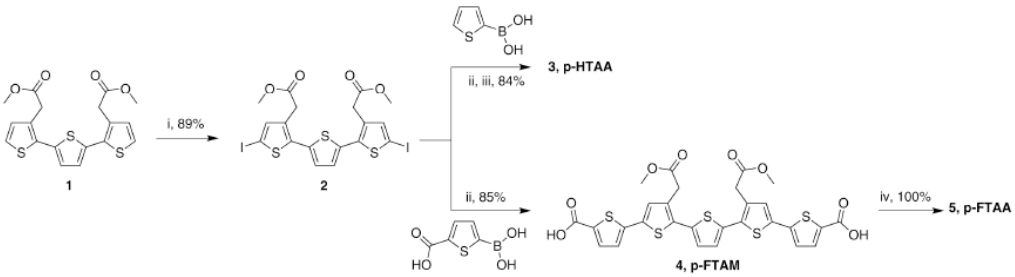

Scheme 1.

Reagents and conditions: (i) NIS, chloroform/acetic acid (1:1); (ii) K_2CO_3, PEPPSI-IPr, toluene/methanol (1:1); (iii) NaOH, H_2O/dioxane (1:1); (iv) NaOH, H_2O